Research Square

Preprints are preliminary reports that have not undergone peer review.
They should not be considered conclusive, used to inform clinical practice,
or referenced by the media as validated information.

How Memory Shape Drives Stability: Gamma Distributed Delays in a Heterogeneous Cournot Duopoly

Luca Guerrini

luca.guerrini@univpm.it

Marche Polytechnic University

Stefania Ragni

University of Ferrara

Research Article

Keywords:

Posted Date: November 18th, 2026

DOI: https://doi.org/10.21203/rs.3.rs-10213336/v1

License: This work is licensed under a Creative Commons Attribution 4.0 International License.
Read Full License

Additional Declarations: No competing interests reported.

How Memory Shape Drives Stability: Gamma Distributed Delays in a Heterogeneous Cournot Duopoly

Luca Guerrini* Stefania Ragni†

Abstract

When firms adjust output with a lag, does the shape of their memory over past observations matter for market stability, or only the average delay? This paper answers the question within a continuous-time heterogeneous Cournot duopoly in which one firm follows a gradient rule and the other a local monopolistic approximation. We replace the conventional fixed point delay with weak and strong Gamma distributed delays and convert the resulting integro-differential system into an exact finite-dimensional representation via the linear chain trick. In the homogeneous-cost benchmark the local system decouples, yielding a complete analytical comparison: the fixed delay is the most destabilizing, the strong Gamma kernel postpones the first Hopf crossing, and the weak Gamma kernel eliminates it entirely. In the heterogeneous-cost case, cost asymmetry activates cross-feedback between the firms, and Hopf thresholds become parameter-dependent. The central conclusion is that stability is governed not only by the mean delay but also by the way past information is distributed over time: the same average lag can be stabilizing or destabilizing depending on whether memory is concentrated at a single date, exponentially decaying, or hump-shaped.

Keywords: heterogeneous duopoly; Gamma distributed delay; linear chain trick; Hopf bifurcation; transversality; Routh–Hurwitz; computational economics

JEL classification: C62, C63, D43, L13

1 Introduction

A fundamental question in oligopoly theory is whether the Nash equilibrium of a quantity-setting game remains stable when firms adjust output dynamically, and what qualitative change marks the transition to instability. Since the foundational work of Cournot [1], this issue has been studied in several dynamic frameworks. In continuous time, implementation lags arise naturally because firms observe market outcomes, process information, and revise production only after a delay. Howroyd and Russell [2] showed early on that such lags may destabilize an otherwise stable equilibrium. Later contributions extended this insight to Cournot duopolies, monopolies and oligopolies by deriving delay-dependent stability conditions, Hopf bifurcation thresholds and stability-switching curves for different market structures and adjustment rules [3, 4, 5, 6, 7, 8]. The monograph by Matsumoto and Szidarovszky [9] provides a systematic treatment of dynamic oligopoly models with time delays.

A complementary stream studies discrete-time oligopoly dynamics with bounded rationality, heterogeneous expectations and adaptive rules. These papers show that even simple output-adjustment mechanisms may generate flip bifurcations, Neimark–Sacker bifurcations, invariant cycles and chaotic trajectories. The early contributions of Puu [13], Agiza and Elsadany [10], Bischi, Naimzada and Sbragia [11], and Tramontana [14] established several benchmark mechanisms through which heterogeneous firms can lose stability. More recent analyses develop this line by

*Department of Management, Polytechnic University of Marche, Ancona, Italy. Email: luca.guerrini@univpm.it
†Department of Economics and Management, University of Ferrara, Ferrara, Italy. Email: stefania.ragni@unife.it

studying evolutionary oligopoly structures, relative-profit objectives, global dynamics, learning behavior and nonlinear game-theoretic formulations [12, 18, 17, 16, 19, 20, 21]. Related recent work on Cournot–Bertrand competition confirms that bifurcation and chaos control remain central issues in heterogeneous market dynamics [15]. Taken together, the continuous- and discrete-time literatures show that instability is not merely an artefact of one timing convention, but a robust consequence of strategic quantity adjustment when firms react to delayed or imperfectly processed information.

The continuous-time benchmark for our analysis is the heterogeneous duopoly of Brianzoni, Campisi and Guerrini [5], which reformulates the delayed model of Tramontana [14]. In that framework, one firm follows a gradient-based boundedly rational rule, whereas the other uses a local monopolistic approximation. This behavioral heterogeneity makes the model especially suitable for studying how delayed information affects market stability. Because the fixed-delay formulation leads to transcendental characteristic equations, its local dynamics are naturally studied with Hopf bifurcation theory for delay differential equations [22, 23], stability-switching methods [6, 24], and geometric criteria for delay-dependent parameters [25]. Related continuous-time delayed Cournot models further show that market dynamics may change qualitatively when output adjustment is no longer instantaneous [26, 27, 28].

A fixed point delay, however, imposes a strong assumption: all information used by a firm at a given date has exactly the same age. In practice, firms aggregate observations arriving over a range of past dates, with recent signals typically carrying more weight than distant ones. This motivates the use of distributed delays, in which the point-delay operator $q(t-\tau)$ is replaced by a weighted average $\int_0^\infty K(s;\tau)q(t-s)\,ds$ with a memory kernel K. Gamma kernels are a natural choice because they allow different memory profiles while preserving a common mean delay. The exponential, or shape-one, kernel represents monotone-decreasing weight on the past, whereas the Erlang, or shape-two, kernel produces a hump-shaped profile concentrated around a preferred lag. Therefore, weak and strong Gamma kernels make it possible to separate the effect of the average delay from the effect of the shape of memory.

A key technical advantage of integer-shape Gamma kernels is that the resulting integro-differential system admits an exact finite-dimensional realization through the linear chain trick. This method, originally due to Fargue [29], was later developed in the theory of distributed-delay systems and structured dynamical models [30, 31, 32, 33, 34, 35]. The chain trick replaces the infinite-dimensional memory operator with auxiliary variables, so that local stability is governed by ordinary characteristic polynomials rather than transcendental equations. This is the reason why Routh–Hurwitz analysis and direct numerical eigenvalue computation can be used throughout the paper.

Distributed-delay methods have been widely used in population dynamics and epidemiology, where memory represents incubation, maturation or distributed response times [31, 34, 36]. In economic dynamics, Gamma kernels have been applied to Cournot games with adjustment frictions and delayed market reactions [3, 4, 7, 8, 37, 38], as well as to duopoly models with multiple distributed lags [39]. Bianca, Guerrini and Ragni [40] used Gamma kernels in an energy demand–supply model, showing how the chain representation makes stability calculations tractable. Wang, Gu, Liu and Xu [41] derived Hopf thresholds for a fractional-order Cournot–Bertrand model with delays. The present paper is also related to the stability-switching analysis of Pecora and Sodini [6], to the bifurcation and chaos-control study of Ahmed, Qureshi, Abbas and Mumtaz [15], and to discrete-time extensions of heterogeneous duopoly dynamics such as Culda, Kaslik, Neamţu and Sîrghi [42].

Our contribution goes beyond replacing one delay specification with another. We provide a systematic comparison of three memory mechanisms, point delay, weak Gamma kernel, and strong Gamma kernel, on the same equilibrium and parameter basis, and we show precisely how the local feedback structure changes when information is distributed over past observations. The comparison produces three main results. First, in the homogeneous-cost case the weak

Gamma kernel is stabilizing for every mean delay, whereas the strong Gamma kernel and the point-delay model lose stability through transversal imaginary-root crossings. Second, in the heterogeneous-cost case cost asymmetry reintroduces cross-feedback between the two firms, so that Hopf thresholds become parameter-dependent and must be obtained from the exact characteristic polynomials or the equivalent chain matrices. Third, the same mean delay can be stabilizing or destabilizing depending on whether the memory is concentrated at one lag, exponentially decreasing, or hump-shaped.

The paper is organized as follows. Section 2 introduces the economic model and the exact Gamma-chain representation. Section 3 derives the corrected local characteristic equation from the Jacobian of the nonlinear rules. Section 4 gives the complete homogeneous-cost Hopf and transversality calculations. Section 5 extends the Hopf tests to heterogeneous marginal costs. Sections 6–7 describe the computational protocol and interpret the numerical results. Sections 8–9 discuss the economic implications and offer concluding remarks.

2 The model and exact Gamma chains

Before turning to the calculations, we first recall the economic model and then show how the distributed-memory terms are converted into finite-dimensional chains. This bridge is useful because every stability statement below will be obtained from the same linearized feedback structure. Let $q_i(t)$ denote the output of firm $i \in \{1,2\}$ at time t. The fixed-delay benchmark system, following [5, 14], is

$$\dot{q}_1(t) = \frac{\alpha_1}{\sigma_1} q_1(t-\tau_1)\left[\frac{q_2(t-\tau_1)}{(q_1(t-\tau_1)+q_2(t-\tau_1))^2} - c_1\right], \tag{1}$$

$$\dot{q}_2(t) = -\frac{1}{\sigma_2} q_2(t) + \frac{1}{\sigma_2}\left[\sqrt{\frac{q_1(t-\tau_2)}{c_2}} - q_1(t-\tau_2)\right]. \tag{2}$$

Here $c_i > 0$ are marginal costs, $\alpha_1 > 0$ is the adjustment speed of firm 1, $\sigma_i > 0$ are adjustment frictions, and $\tau_i \geq 0$ are time delays. Firm 1 uses a gradient-based (bounded rationality) rule: it adjusts output in the direction of the estimated marginal profit $q_2/(q_1+q_2)^2 - c_1$, scaled by the current output level and the adjustment speed. Firm 2 uses a local monopolistic approximation: it targets the best-response output $\sqrt{q_1/c_2} - q_1$ with an inertia parameter σ_2. This heterogeneity in decision mechanisms is the central feature of the model. For a unit-mass memory kernel $K_i(s;\tau_i)$, define the memory operator

$$(\mathcal{M}_{K_i} q_j)(t) = \int_0^\infty K_i(s;\tau_i) q_j(t-s)\, ds.$$

The distributed-memory extension replaces each delayed signal $q_j(t-\tau_i)$ by its memory average $(\mathcal{M}_{K_i} q_j)(t)$. Since every kernel has unit mass, the positive Nash equilibrium is unchanged:

$$E = (E_1, E_2) = \left(\frac{c_2}{(c_1+c_2)^2}, \frac{c_1}{(c_1+c_2)^2}\right).$$

We compare the shape-one (weak) and shape-two (strong) Gamma profiles with common mean delay τ:

$$K_{\mathrm{w}}(s;\tau) = \frac{1}{\tau} e^{-s/\tau}, \qquad K_{\mathrm{s}}(s;\tau) = \frac{4s}{\tau^2} e^{-2s/\tau}, \qquad s \geq 0.$$

Both are unit-mass distributions with mean τ. For the weak kernel, $z_j = \mathcal{M}_{K_{\mathrm{w}}} q_j$ satisfies the first-order chain

$$\dot{z}_j = \frac{q_j - z_j}{\tau}, \qquad j = 1, 2.$$

For the strong kernel, $z_{j,2} = \mathcal{M}_{K_s} q_j$ is generated by the second-order chain

$$\dot{z}_{j,1} = \frac{2}{\tau}(q_j - z_{j,1}), \qquad \dot{z}_{j,2} = \frac{2}{\tau}(z_{j,1} - z_{j,2}), \qquad j = 1, 2. \tag{3}$$

These chain systems are exact representations of the Gamma convolutions, not approximations [31, 32, 33, 34, 35].

3 Linearization and characteristic equations

We now pass from the nonlinear economic rules to the local system that determines stability. The following computation is the point at which the correction with respect to the benchmark paper enters. Put $u_i = q_i - E_i$. Direct differentiation of the right-hand sides of (1)–(2) at E gives the linearization coefficients

$$p = \frac{2\alpha_1 c_1 c_2}{\sigma_1(c_1 + c_2)} > 0, \qquad b = \frac{\alpha_1 c_2(c_2 - c_1)}{\sigma_1(c_1 + c_2)},$$
$$\gamma = \frac{c_1 - c_2}{2c_2\sigma_2}, \qquad A = \frac{1}{\sigma_2} > 0,$$
$$d = -b\gamma = \frac{\alpha_1(c_1 - c_2)^2}{2\sigma_1\sigma_2(c_1 + c_2)} \geq 0.$$

The linearized distributed-memory system takes the form

$$\dot{u}_1 = -p\,\mathcal{M}_K u_1 + b\,\mathcal{M}_K u_2, \qquad \dot{u}_2 = -Au_2 + \gamma\,\mathcal{M}_K u_1. \tag{4}$$

If $H(\lambda)$ denotes the Laplace transform of the kernel K, the associated characteristic equation is

$$\Delta(\lambda) = (\lambda + pH(\lambda))(\lambda + A) + dH(\lambda)^2 = 0. \tag{5}$$

Expanding,

$$\lambda^2 + A\lambda + (pA + p\lambda)H(\lambda) + dH(\lambda)^2 = 0. \tag{6}$$

The coefficient multiplying $\lambda H(\lambda)$ is $p > 0$, fixed by the Jacobian of the nonlinear system.

4 Complete homogeneous-cost theory

The homogeneous case is the cleanest benchmark because the cross-coupling terms vanish. We analyze it first in full detail; this gives explicit thresholds against which the heterogeneous case can later be compared. Assume $c_1 = c_2 = c$. Then $b = \gamma = d = 0$ and (5) factorizes as

$$(\lambda + A)(\lambda + pH(\lambda)) = 0, \qquad p = \frac{\alpha_1 c}{\sigma_1} > 0.$$

The root $\lambda = -A < 0$ is stable; all local stability information is contained in the scalar factor $\lambda + pH(\lambda) = 0$.

4.1 Fixed point delay

For $H(\lambda) = e^{-\lambda\tau}$, the nontrivial factor is

$$F(\lambda, \tau) = \lambda + pe^{-\lambda\tau} = 0. \tag{7}$$

Theorem 1 (Fixed-delay Hopf crossings)**.** *Let $p > 0$. The homogeneous fixed-delay system is locally asymptotically stable for $0 \le \tau < \tau_{\mathrm{d},0}$, where*

$$\tau_{\mathrm{d},k} = \frac{(2k+1)\pi}{2p}, \qquad k = 0, 1, 2, \dots. \tag{8}$$

At every $\tau_{\mathrm{d},k}$, the characteristic equation has the simple pair $\lambda = \pm ip$, and the transversality condition holds:

$$\left.\frac{d\,\mathrm{Re}\,\lambda}{d\tau}\right|_{\tau=\tau_{\mathrm{d},k}} = \frac{p^2}{1 + p^2\tau_{\mathrm{d},k}^2} > 0. \tag{9}$$

Proof. Setting $\lambda = i\omega$ in (7) and separating real and imaginary parts gives $p\cos(\omega\tau) = 0$ and $\omega - p\sin(\omega\tau) = 0$. The first equation yields $\omega\tau = (2k+1)\pi/2$; substitution into the second gives $\omega = p$, whence (8). For transversality, the partial derivatives of F are $F_\lambda = 1 - p\tau e^{-\lambda\tau}$ and $F_\tau = -p\lambda e^{-\lambda\tau}$. Implicit differentiation yields

$$\frac{d\lambda}{d\tau} = -\frac{F_\tau}{F_\lambda} = \frac{p\lambda e^{-\lambda\tau}}{1 - p\tau e^{-\lambda\tau}}.$$

At $\lambda = ip$ and $\tau = \tau_{\mathrm{d},k}$, this reduces to $d\lambda/d\tau = p^2/(1 + ip\tau_{\mathrm{d},k})$. Taking real parts gives (9). Since $F_\lambda = 1 + ip\tau_{\mathrm{d},k} \neq 0$, the root is simple. □

4.2 Weak Gamma memory

For $H_{\mathrm{w}}(\lambda) = (1 + \tau\lambda)^{-1}$, the nontrivial factor becomes

$$P_{\mathrm{w}}^{\mathrm{h}}(\lambda, \tau) = \tau\lambda^2 + \lambda + p = 0. \tag{10}$$

Theorem 2 (Weak Gamma stability)**.** *For every $p > 0$ and every $\tau > 0$, all roots of (10) have strictly negative real part. Hence the homogeneous weak-Gamma system has no Hopf crossing as the mean delay varies.*

Proof. The polynomial (10) has coefficients $\tau > 0$, $1 > 0$, and $p > 0$. By the Routh–Hurwitz criterion for a quadratic, all roots have negative real part if and only if every coefficient is positive, which holds for every $\tau > 0$. □

4.3 Strong Gamma memory

For $H_{\mathrm{s}}(\lambda) = (1 + \tau\lambda/2)^{-2}$, the scalar factor is

$$P_{\mathrm{s}}^{\mathrm{h}}(\lambda, \tau) = \frac{\tau^2}{4}\lambda^3 + \tau\lambda^2 + \lambda + p = 0. \tag{11}$$

Theorem 3 (Strong Gamma Hopf crossing)**.** *Let $p > 0$. The homogeneous strong-Gamma system is locally asymptotically stable for $0 < \tau < \tau_{\mathrm{s}}^*$, where*

$$\tau_{\mathrm{s}}^* = \frac{4}{p}.$$

At $\tau = \tau_{\mathrm{s}}^*$ there is a simple pair $\lambda = \pm i\omega_{\mathrm{s}}$ with

$$\omega_{\mathrm{s}} = \frac{p}{2},$$

and the crossing is transversal:

$$\left.\frac{d\,\mathrm{Re}\,\lambda}{d\tau}\right|_{\tau=\tau_{\mathrm{s}}^*} = \frac{p^2}{40} = \frac{2}{5(\tau_{\mathrm{s}}^*)^2} > 0.$$

Proof. Write the cubic (11) as $a_3\lambda^3 + a_2\lambda^2 + a_1\lambda + a_0 = 0$ with $a_3 = \tau^2/4$, $a_2 = \tau$, $a_1 = 1$, $a_0 = p$. All coefficients are positive. The cubic Routh–Hurwitz necessary and sufficient condition for stability is $a_2a_1 - a_3a_0 > 0$, that is, $\tau \cdot 1 - (\tau^2/4) \cdot p > 0$, equivalently $\tau < 4/p$. At the boundary $\tau = 4/p$, the Routh–Hurwitz determinant vanishes and a pair of purely imaginary roots exists. Substituting $\lambda = i\omega$ into (11) and separating real and imaginary parts:

$$\text{Real:} \quad -\tau\omega^2 + p = 0, \qquad \text{Imaginary:} \quad \omega - \frac{\tau^2}{4}\omega^3 = 0.$$

The real equation gives $\omega^2 = p/\tau = p^2/4$, hence $\omega = p/2$. One verifies that the imaginary equation is also satisfied at $\tau = 4/p$ and $\omega = p/2$. Let $P = P_{\mathrm{s}}^{\mathrm{h}}$. The derivatives are $P_\lambda = \frac{3\tau^2}{4}\lambda^2 + 2\tau\lambda + 1$ and $P_\tau = \frac{\tau}{2}\lambda^3 + \lambda^2$. At $\tau = 4/p$ and $\lambda = ip/2$:

$$P_\lambda = \frac{3\tau^2}{4}\left(-\frac{p^2}{4}\right) + 2\tau \cdot \frac{ip}{2} + 1 = -3 + 4i + 1 = -2 + 4i,$$

which is nonzero, confirming simplicity. Implicit differentiation gives $d\lambda/d\tau = -P_\tau/P_\lambda$. Indeed, at the critical point

$$P_\tau = \frac{\tau}{2}\lambda^3 + \lambda^2 = -\frac{p^2}{4}(1+i), \qquad -\frac{P_\tau}{P_\lambda} = \frac{p^2(1+i)}{4(-2+4i)} = \frac{p^2}{40}(1-3i).$$

Therefore $\mathrm{Re}(d\lambda/d\tau) = p^2/40 > 0$. □

5 General heterogeneous-cost Hopf conditions

We next remove the simplifying assumption of equal costs. The calculations are less compact, but the same Hopf logic applies: one first finds imaginary roots, then checks that they are simple and transversal. Assume $c_1 \neq c_2$, so $d > 0$ and the two firms are locally coupled through the cross-feedback terms b and γ in (4). Closed-form thresholds are generally unavailable, but the following results provide complete, parameter-dependent Hopf tests for all three memory specifications.

5.1 Fixed delay

For $H(\lambda) = e^{-\lambda\tau}$, define

$$\Delta_{\mathrm{d}}(\lambda, \tau) = (\lambda + pe^{-\lambda\tau})(\lambda + A) + de^{-2\lambda\tau}. \tag{12}$$

For $\lambda = i\omega$ and $\theta = \omega\tau$, the necessary conditions for a purely imaginary root are

$$\begin{aligned} R_{\mathrm{d}}(\omega, \tau) &= -\omega^2 + p(A\cos\theta + \omega\sin\theta) + d\cos(2\theta) = 0, \\ I_{\mathrm{d}}(\omega, \tau) &= A\omega + p(\omega\cos\theta - A\sin\theta) - d\sin(2\theta) = 0. \end{aligned}$$

5.2 Weak Gamma kernel

After multiplication by $(1 + \tau\lambda)^2$, the exact weak-Gamma characteristic polynomial is

$$\begin{aligned} P_{\mathrm{w}}(\lambda, \tau) = \tau^2\lambda^4 + \tau(2 + A\tau)\lambda^3 + [1 + \tau(2A + p)]\lambda^2 \\ + [A + p + pA\tau]\lambda + (pA + d). \end{aligned} \tag{13}$$

Writing $P_{\mathrm{w}} = a_4\lambda^4 + a_3\lambda^3 + a_2\lambda^2 + a_1\lambda + a_0$, all coefficients are positive for every $\tau > 0$. The Routh–Hurwitz conditions for a quartic reduce to two nontrivial determinantal inequalities:

$$\Delta_2 = a_3a_2 - a_4a_1 > 0, \tag{14}$$

$$\Delta_3 = a_3a_2a_1 - a_4a_1^2 - a_3^2a_0 > 0. \tag{15}$$

Since all $a_j > 0$, conditions (14)–(15) are necessary and sufficient for local stability. For a potential Hopf point, $\omega > 0$ and $\tau > 0$ must satisfy

$$R_{\mathrm{w}}(\omega, \tau) = \tau^2\omega^4 - [1 + \tau(2A + p)]\omega^2 + pA + d = 0, \tag{16}$$

$$I_{\mathrm{w}}(\omega, \tau) = -\tau(2 + A\tau)\omega^3 + [A + p + pA\tau]\omega = 0. \tag{17}$$

From (17), the Hopf frequency satisfies

$$\omega^2 = \frac{A + p + pA\tau}{\tau(2 + A\tau)}. \tag{18}$$

Substitution of (18) into (16) gives a single scalar condition in τ that determines the Hopf threshold implicitly.

5.3 Strong Gamma kernel

Let $L(\lambda, \tau) = (1 + \tau\lambda/2)^2$. The exact strong-Gamma characteristic polynomial is the degree-six polynomial

$$P_{\mathrm{s}}(\lambda, \tau) = (\lambda L(\lambda, \tau) + p)(\lambda + A)L(\lambda, \tau) + d. \tag{19}$$

Its stability is equivalent to positivity of the six Hurwitz determinants of P_{s}. For an explicit Hopf test, put $x = \tau\omega/2$, $\ell_r = 1 - x^2$, $\ell_i = 2x$, and define $M_r = p - \tau\omega^2$, $M_i = \omega\ell_r$, $N_r = A(1 - \tau^2\omega^2/4) - \tau\omega^2$, $N_i = \omega(1 + A\tau - \tau^2\omega^2/4)$. Then $\lambda = i\omega$ is a root exactly when

$$R_{\mathrm{s}}(\omega, \tau) = M_rN_r - M_iN_i + d = 0,$$
$$I_{\mathrm{s}}(\omega, \tau) = M_rN_i + M_iN_r = 0.$$

Proposition 4 (General transversal Hopf test)**.** *For $j \in \{\mathrm{d}, \mathrm{w}, \mathrm{s}\}$, let Δ_j denote respectively (12), (13), or (19). Suppose that (ω^*, τ^*) with $\omega^* > 0$ solves the corresponding real and imaginary equations. If*

$$\partial_\lambda\Delta_j(i\omega^*, \tau^*) \neq 0, \qquad \mathrm{Re}\left[-\frac{\partial_\tau\Delta_j(i\omega^*, \tau^*)}{\partial_\lambda\Delta_j(i\omega^*, \tau^*)}\right] \neq 0, \tag{20}$$

then the pair $\pm i\omega^*$ is simple and crosses the imaginary axis transversally as τ passes through τ^*.

Proof. The implicit-function theorem applies to the simple root because $\partial_\lambda\Delta_j \neq 0$. Differentiation of $\Delta_j(\lambda(\tau), \tau) = 0$ gives $d\lambda/d\tau = -\partial_\tau\Delta_j/\partial_\lambda\Delta_j$. The second condition in (20) is precisely the nonzero crossing speed. □

For reproducibility, we record the explicit derivatives used in the numerical implementation. For the weak kernel:

$$\partial_\lambda P_{\mathrm{w}} = 4\tau^2\lambda^3 + 3\tau(2 + A\tau)\lambda^2 + 2[1 + \tau(2A + p)]\lambda + A + p + pA\tau,$$

$$\partial_\tau P_{\mathrm{w}} = 2\tau\lambda^4 + (2 + 2A\tau)\lambda^3 + (2A + p)\lambda^2 + pA\lambda.$$

6 Computational protocol

The theoretical conditions above are now implemented numerically using only exact objects: the weak and strong Gamma chains and, for the point-delay comparison, the corresponding characteristic roots. For the weak kernel, the exact chain matrix in variables (u_1, u_2, z_1, z_2) is

$$M_{\mathrm{w}}(\tau) = \begin{pmatrix} 0 & 0 & -p & b \\ 0 & -A & \gamma & 0 \\ \tau^{-1} & 0 & -\tau^{-1} & 0 \\ 0 & \tau^{-1} & 0 & -\tau^{-1} \end{pmatrix}. \tag{21}$$

For the strong kernel, (3) yields the 6×6 exact matrix in variables $(u_1, u_2, z_{1,1}, z_{2,1}, z_{1,2}, z_{2,2})$:

$$M_{\mathrm{s}}(\tau) = \begin{pmatrix} 0 & 0 & 0 & 0 & -p & b \\ 0 & -A & 0 & 0 & \gamma & 0 \\ r & 0 & -r & 0 & 0 & 0 \\ 0 & r & 0 & -r & 0 & 0 \\ 0 & 0 & r & 0 & -r & 0 \\ 0 & 0 & 0 & r & 0 & -r \end{pmatrix}, \qquad r = \frac{2}{\tau}. \tag{22}$$

The spectral abscissa is $\mathrm{sa}(M) = \max\{\mathrm{Re}\,\lambda : \lambda \in \mathrm{spec}(M)\}$. The Python script accompanying this paper computes all eigenvalues directly from M_{w} and M_{s}, evaluates the fixed-delay homogeneous spectrum via the Lambert-W function [43], integrates the full nonlinear chain systems by adaptive Runge–Kutta methods, and generates every figure and table.

7 Numerical illustrations

This section presents a set of numerical experiments designed to illustrate the theoretical results established in the previous sections. We first consider a homogeneous benchmark, which provides a reference configuration for interpreting the dynamic properties of the model. The subsequent numerical examples then investigate how different memory structures and parameter values affect local stability, the onset of oscillatory dynamics, and the emergence of Hopf bifurcations. Throughout the section, the simulations complement the analytical findings by providing an intuitive visualization of the qualitative behavior predicted by the theoretical analysis.

7.1 Homogeneous benchmark

We begin with the homogeneous calibration because it allows the figures to be read directly against the closed-form thresholds derived in Section 4. We adopt the benchmark parameters

$$\sigma_1 = 0.81, \quad \sigma_2 = 0.74, \quad \alpha_1 = 1, \quad c_1 = c_2 = 0.69. \tag{23}$$

These are the same values used in [5] to facilitate direct comparison. The derived quantities are listed in Table 1.

Table 1: Homogeneous-cost derived quantities ($c_1 = c_2 = 0.69$).

Parameter	Formula	Value
p	$2\alpha_1 c_1 c_2/[\sigma_1(c_1+c_2)]$	0.851852
A	$1/\sigma_2$	1.351351
$E_1 = E_2$	$c/(2c)^2 = 1/(4c)$	0.362319
$\tau_{\mathrm{d},0}$	$\pi/(2p)$	1.843978
τ_{s}^*	$4/p$	4.695652
ω_{s}	$p/2$	0.425926
$d\,\mathrm{Re}\,\lambda/d\tau\vert_{\mathrm{fixed},k=0}$	$p^2/(1+p^2\tau_{\mathrm{d},0}^2)$	0.209278
$d\,\mathrm{Re}\,\lambda/d\tau\vert_{\mathrm{strong}}$	$p^2/40$	0.018141

Figure 1 shows the spectral abscissa as a function of the mean delay τ for all three specifications, confirming the analytical ranking: fixed delay loses stability first (at $\tau_{\mathrm{d},0} \approx 1.844$), strong Gamma memory later (at $\tau_{\mathrm{s}}^* \approx 4.696$), and weak Gamma memory remains stable over the entire range. The reference [5] reports a Hopf bifurcation at $\tau \approx 1.77$ for the same parameter set with fixed delay.

Table 2 provides a detailed comparison between the stability results obtained with the original linearization of [5] (fixed point delay only, coefficient $C = -1$) and the corrected linearization

used here (coefficient $p > 0$). The corrected form shifts the homogeneous Hopf threshold upward and, more importantly, opens the analysis to the weak and strong Gamma specifications for which the linear chain trick provides exact polynomial characteristic equations.

Table 2: Comparison between the fixed-delay analysis in Brianzoni et al. [5] and the present corrected analysis ($c_1 = c_2 = 0.69$, $\sigma_1 = 0.81$, $\sigma_2 = 0.74$, $\alpha_1 = 1$).

	Brianzoni et al. [5]	Present (fixed delay)	Difference
Linearization coefficient	$C = -1$	$p = 0.852$	Corrected Jacobian
Hopf threshold τ^*	≈ 1.77	1.844	+4.2%
Hopf frequency ω^*	≈ 1.74	$p = 0.852$	Different formula
Transversality	Verified	Verified (eq. (9))	—
Delay-free stability	$\sigma_2 < 1$	$\sigma_2 < 1$	Same
Equilibrium E	$(0.362, 0.362)$	$(0.362, 0.362)$	Same

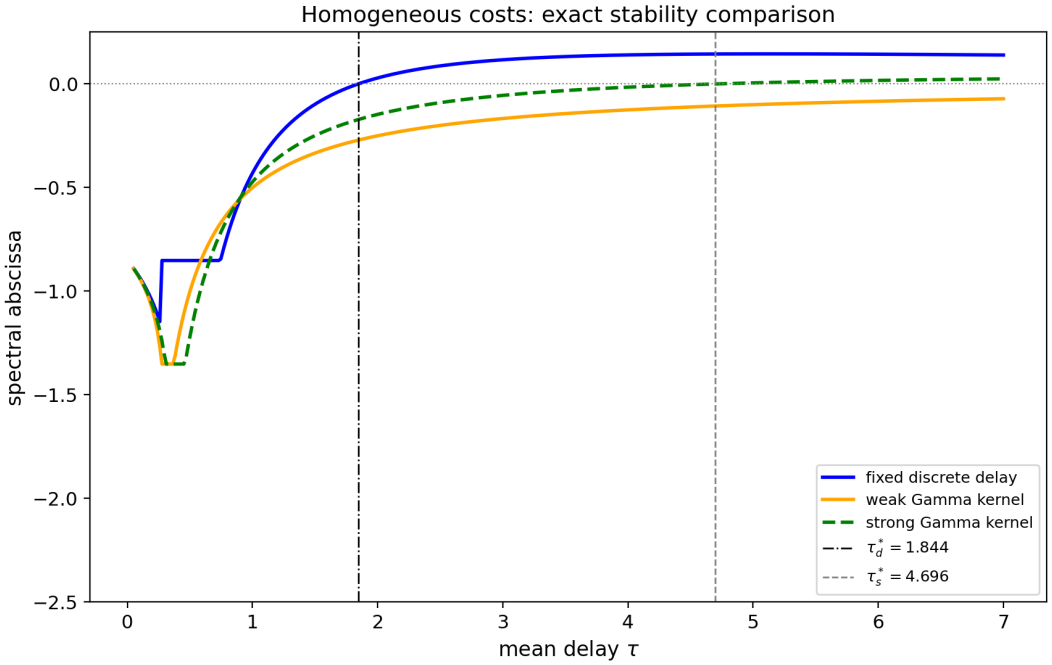


Figure 1: Homogeneous-cost spectral abscissa versus mean delay τ. Curves are computed from the exact Gamma-chain matrices (21)–(22) and the Lambert-W representation for the fixed delay. Vertical lines mark the analytical thresholds $\tau_{\mathrm{d},0}$ and τ_{s}^*.

Economically, Figure 1 says that a firm reacting to a single dated signal is the most exposed to oscillatory overreaction. Once the same information is spread over a memory distribution, the destabilizing feedback is filtered. The weak Gamma curve remains below zero because recent observations dominate the adjustment rule; the strong Gamma curve eventually crosses zero because its hump-shaped memory still gives substantial weight to a preferred past lag.

Figure 2 illustrates the weak and strong Gamma kernels for three values of τ. The two kernels share the same mean delay but differ in the temporal concentration of weight: the weak kernel places maximal weight on the present, while the strong kernel concentrates weight around a preferred lag.

The interpretation of Figure 2 is important for the economic comparison. The fixed delay corresponds to the limiting case in which all weight is concentrated at one date. The weak kernel describes gradual forgetting, while the strong kernel describes a production or information

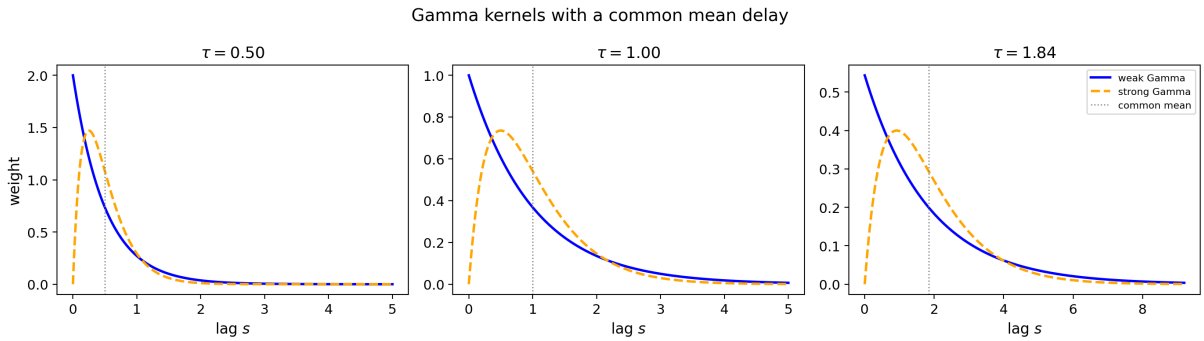


Figure 2: Weak and strong Gamma kernels with identical mean delay τ.

process with a most relevant past date. Thus, the following stability differences are caused by memory shape and not by a change in the mean delay.

Figure 3 displays the dominant linear modes for the three specifications, illustrating the time-domain signatures of stability (decaying oscillations) and instability (growing oscillations).

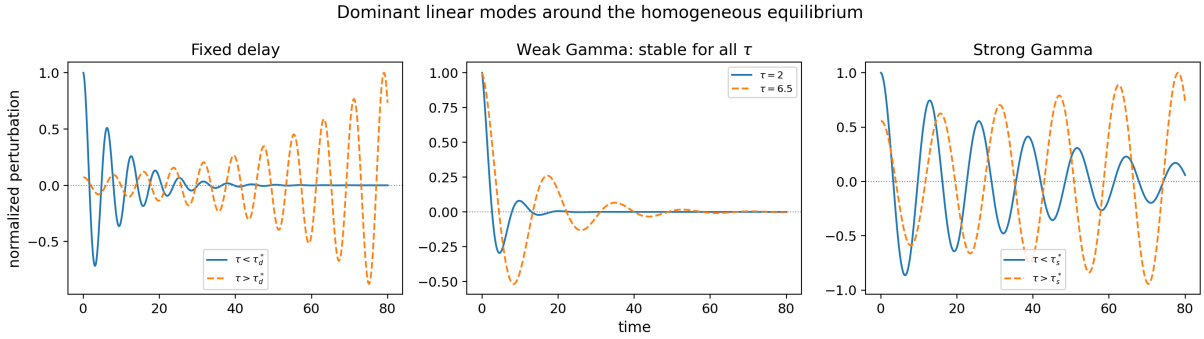


Figure 3: Dominant linear modes around the homogeneous equilibrium. These are computed from the analytical eigenvalues, not from nonlinear simulations.

Figure 3 translates the eigenvalue calculations into time-domain language. When the dominant real part is negative, deviations from the Nash equilibrium are damped. When it is positive, the same type of oscillation is amplified. This makes clear why the sign of the spectral abscissa is the central diagnostic used in the numerical part.

Figure 4 provides a numerical verification of the transversality formula in Theorem 3. The left panel shows that $\mathrm{Re}\,\lambda_+(\tau)$ crosses zero with positive slope at $\tau = \tau_s^*$; the analytically predicted slope $p^2/40 = 0.01814$ matches the centered-difference computation to five significant digits. The right panel shows the root-locus diagram, confirming that one pair of roots crosses the imaginary axis as τ increases through τ_s^*.

Figure 4 is the numerical counterpart of the analytical transversality calculation. The crossing is not tangential: the real part passes through zero with positive slope. Hence the loss of local stability is robust with respect to small changes in the delay parameter.

Figure 5 presents the bifurcation diagram for the strong Gamma specification in the homogeneous case, obtained by integrating the full nonlinear chain system and recording the extrema of $q_1(t)$ after transient removal. The transition from a stable equilibrium to oscillatory dynamics at $\tau \approx \tau_s^*$ is clearly visible.

Figure 5 should be read as a nonlinear diagnostic rather than as an additional proof of Hopf direction. Below the threshold, all recorded extrema collapse to the equilibrium value. Above the threshold, several extrema appear, indicating persistent oscillations in output. This supports the local spectral prediction that the equilibrium is no longer attracting.

Figure 6 shows the phase-plane attractors for the same homogeneous strong Gamma system

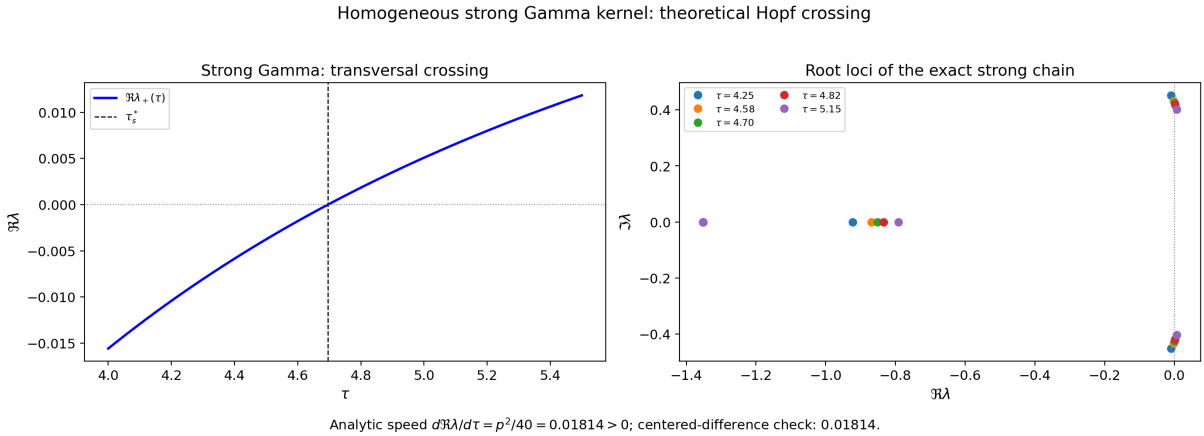


Figure 4: Strong Gamma kernel: numerical verification of Theorem 3.

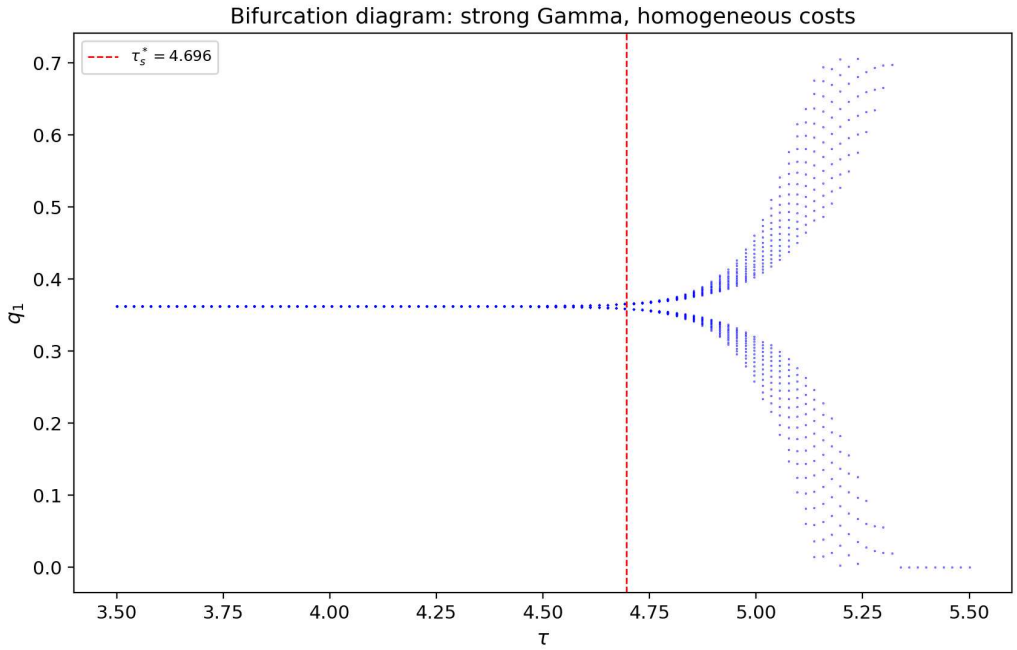


Figure 5: Bifurcation diagram for the strong Gamma chain in the homogeneous case. Extrema of q_1 are plotted after transient removal.

at two delay values above the threshold. At $\tau = 4.85$, just above τ_s^*, the trajectory converges to a simple closed orbit surrounding the unstable Nash equilibrium. At $\tau = 5.2$, the attractor develops a more complex shape, consistently with the bifurcation structure visible in Figure 5. These phase portraits are analogous to those reported in [5, Figures 2–3] for the fixed-delay specification.

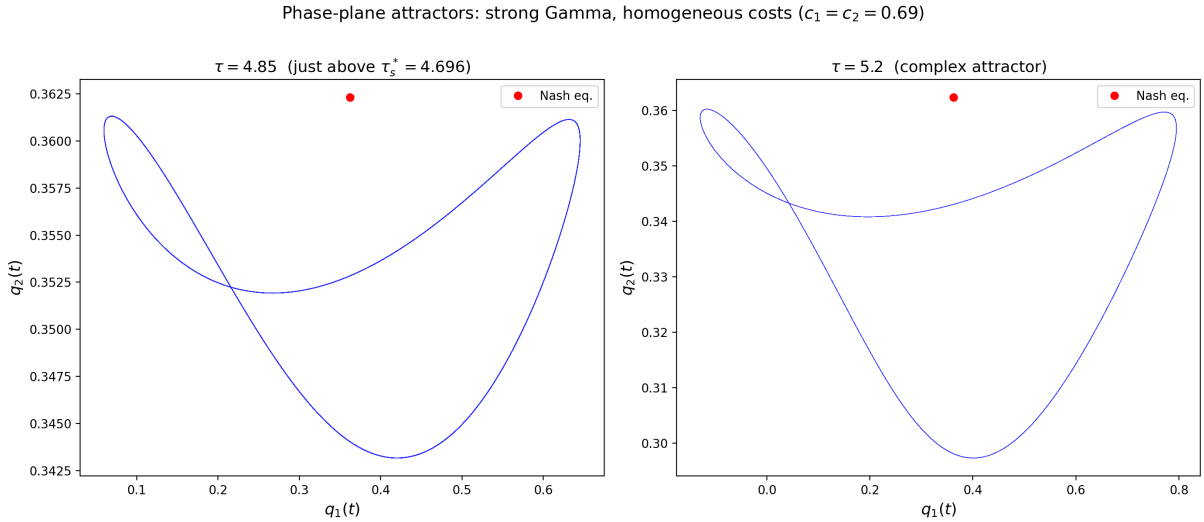


Figure 6: Phase-plane attractors for the strong Gamma chain, homogeneous costs. Left: simple limit cycle near the Hopf crossing; right: complex attractor at larger τ.

The phase portraits in Figure 6 show what the oscillations mean in market terms. The two firms do not simply move independently away from equilibrium; their outputs rotate around the Nash point. Near the threshold the motion is regular, while for larger delays the orbit becomes more distorted, suggesting that stronger memory-induced feedback may generate richer nonlinear behavior.

7.2 Heterogeneous costs

The previous figures isolate memory shape when the firms have the same marginal cost. We now keep the same adjustment parameters but introduce cost asymmetry, so that the cross-feedback terms become active. For the heterogeneous illustration we set $c_1 = 3$ and $c_2 = 0.2$, keeping the remaining values in (23). This is a deliberately asymmetric configuration chosen so that both the weak and strong Gamma systems exhibit a crossing on the explored interval. Table 3 summarizes the derived parameters.

Table 3: Heterogeneous-cost derived quantities ($c_1 = 3$, $c_2 = 0.2$).

Parameter	Formula	Value
p	$2\alpha_1 c_1 c_2/[\sigma_1(c_1+c_2)]$	0.462963
b	$\alpha_1 c_2(c_2-c_1)/[\sigma_1(c_1+c_2)]$	-0.216049
γ	$(c_1-c_2)/(2c_2\sigma_2)$	9.459459
A	$1/\sigma_2$	1.351351
d	$\alpha_1(c_1-c_2)^2/[2\sigma_1\sigma_2(c_1+c_2)]$	2.043710
E_1	$c_2/(c_1+c_2)^2$	0.019531
E_2	$c_1/(c_1+c_2)^2$	0.292969

Figure 7 reports the spectral abscissae obtained from the exact chain matrices. The numerical

crossings occur near $\tau_w^* \approx 0.858$ (weak) and $\tau_s^* \approx 0.565$ (strong), with the strong kernel destabilizing earlier.

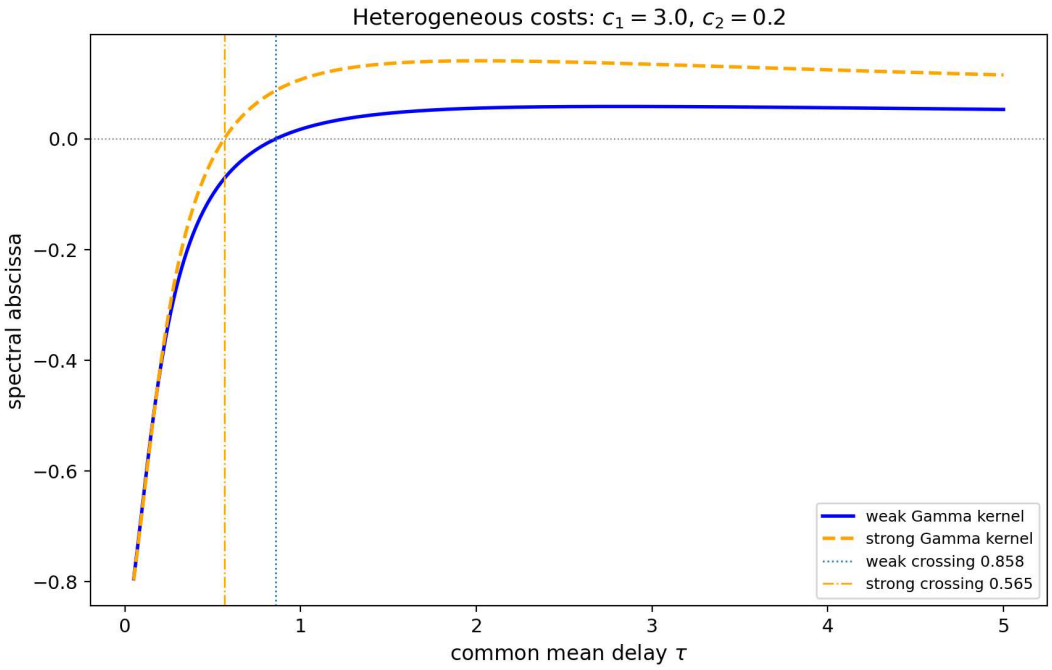


Figure 7: Heterogeneous-cost spectral scans from the exact chain matrices.

Figure 7 shows that cost heterogeneity changes the stabilizing ranking. In the reported asymmetric calibration, the strong kernel destabilizes before the weak kernel. The reason is that cost asymmetry activates the cross term d: feedback from one firm's delayed signal now affects the other firm's adjustment, and the hump-shaped strong kernel can reinforce this cross-feedback more strongly than the exponentially decreasing weak kernel.

Table 4 evaluates the Routh–Hurwitz determinants (14)–(15) of the weak-Gamma quartic (13) at several values of τ. The table confirms that Δ_3 changes sign between $\tau = 0.7$ and $\tau = 0.858$, consistent with the numerically detected crossing.

Table 4: Weak-Gamma Routh–Hurwitz determinants for the heterogeneous case ($c_1 = 3$, $c_2 = 0.2$).

τ	a_4	a_3	a_2	a_1	a_0	Δ_2	Δ_3	Stable?
0.30	0.090	0.722	1.950	2.002	2.669	1.227	1.066	Yes
0.50	0.250	1.338	2.583	2.127	2.669	2.924	1.441	Yes
0.70	0.490	2.062	3.216	2.252	2.669	5.528	1.100	Yes
0.858	0.736	2.711	3.716	2.351	2.669	8.343	≈ 0	Boundary
1.00	1.000	3.351	4.166	2.440	2.669	11.521	−1.871	No
1.50	2.250	6.041	5.749	2.753	2.669	28.530	−18.862	No
2.00	4.000	9.405	7.331	3.066	2.669	56.692	−62.341	No

Table 5 presents an analogous Hurwitz scan for the strong-Gamma degree-six polynomial (19). The leading Hurwitz determinant that changes sign is the fifth (Δ_5), and the sign change occurs between $\tau = 0.5$ and $\tau = 0.565$, consistently with the crossing visible in Figure 7.

Figure 8 evaluates the numerical realization of the general test (20). The left panel shows that both the weak and strong spectral abscissae cross zero with positive slope, confirming transversality. The right panel displays the exact-chain root clouds for several values of τ, showing the passage of eigenvalue pairs through the imaginary axis.

Table 5: Strong-Gamma Hurwitz diagnostics for the heterogeneous case ($c_1 = 3$, $c_2 = 0.2$). The column sa is the spectral abscissa computed from the exact 6×6 chain matrix.

τ	sa(M_s)	Sign of Δ_5	Stable?
0.10	-0.831	$+$	Yes
0.20	-0.621	$+$	Yes
0.30	-0.413	$+$	Yes
0.40	-0.188	$+$	Yes
0.50	-0.046	$+$	Yes
0.565	≈ 0	≈ 0	Boundary
0.60	$+0.014$	$-$	No
0.80	$+0.068$	$-$	No
1.00	$+0.090$	$-$	No

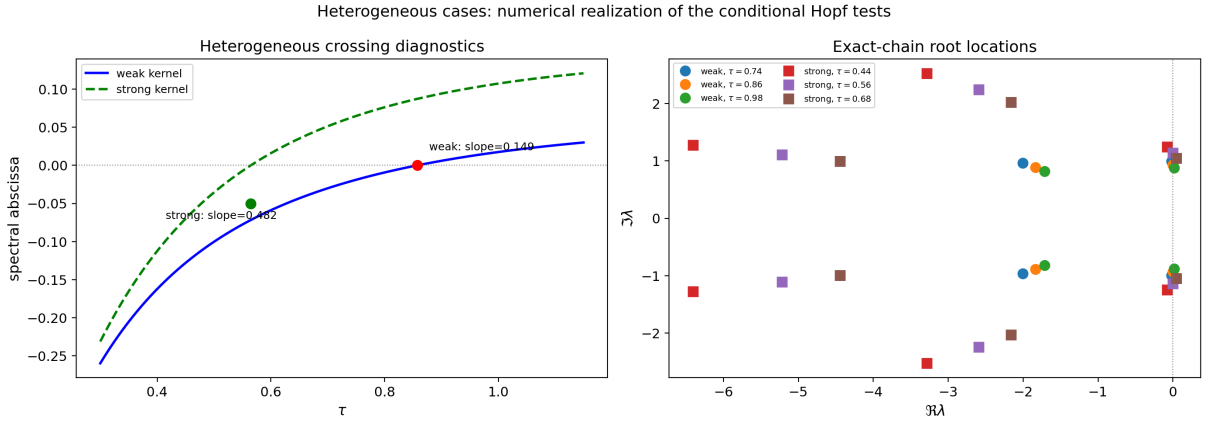


Figure 8: Heterogeneous Hopf test (Proposition 4): crossing diagnostics (left) and exact-chain root locations (right).

Figure 8 gives the geometric reading of the same event. Before the critical delay, the relevant roots lie in the left half-plane. At the critical value they meet the imaginary axis. After the crossing, they enter the right half-plane, producing growing oscillatory deviations from equilibrium.

Figure 9 is a two-parameter stability map in the (τ, α_1) plane. Three regions are identified: stable under both kernels (green), stable under weak but unstable under strong (yellow), and unstable under both (pink). The map shows that increasing either the mean delay or the adjustment speed destabilizes the system, and that the strong kernel is uniformly more susceptible to instability than the weak kernel.

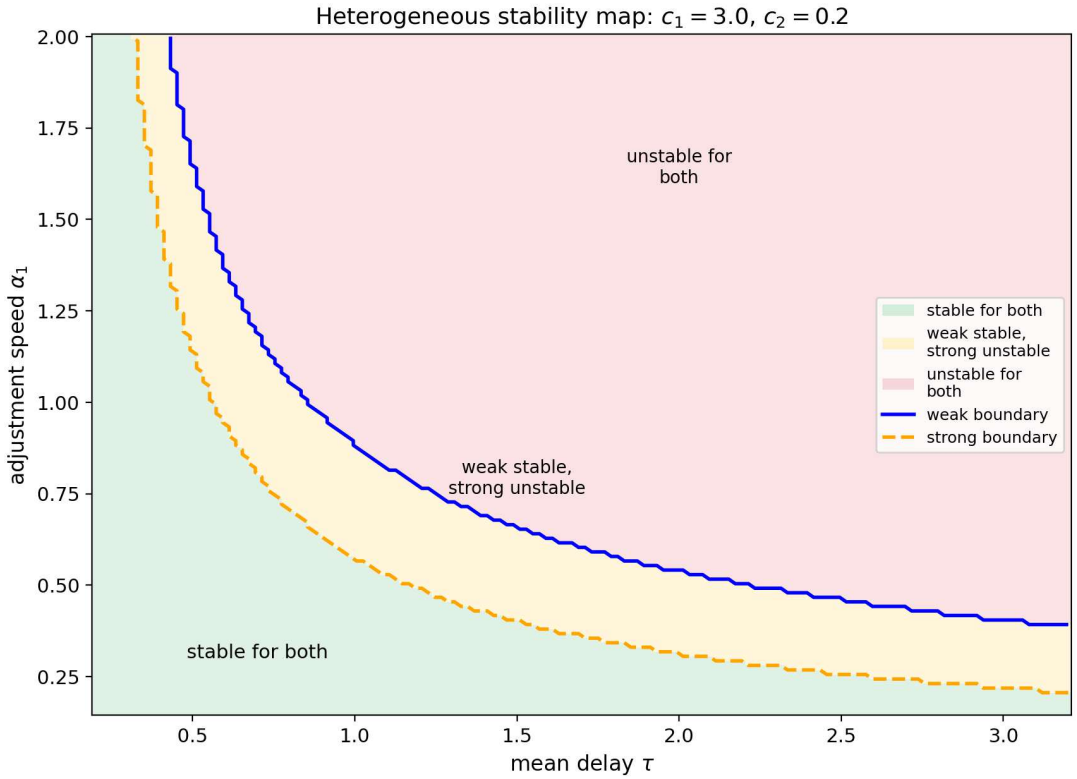


Figure 9: Two-parameter stability map for the heterogeneous case ($c_1 = 3$, $c_2 = 0.2$).

Figure 9 is useful because it separates the effects of memory and adjustment speed. A larger adjustment speed makes firm 1 react more aggressively to perceived profit opportunities; a larger mean delay makes this reaction more outdated. The unstable region expands when these two forces combine.

Figure 10 presents full nonlinear exact-chain diagnostics around the heterogeneous crossings. Below each crossing the perturbation decays, while above it the oscillatory mode grows. These simulations confirm the linear stability predictions but do not determine the first Lyapunov coefficient and therefore do not classify the emerging periodic solutions.

Figure 10 confirms that the local eigenvalue result is visible in the nonlinear chains. Below the crossing, a small perturbation is absorbed by the system. Above it, the perturbation is amplified and becomes oscillatory. This is the economic signature of delayed overadjustment.

Figure 11 shows bifurcation diagrams for both the weak and strong Gamma specifications in the heterogeneous case, plotting the extrema of $q_2(t)$ as a function of τ after transient removal.

Figure 11 completes the heterogeneous-cost comparison. The weak and strong kernels both generate oscillations after their respective thresholds, but the onset occurs at different delays. This illustrates the main message of the paper: the same mean delay can imply different market dynamics depending on the distribution of memory weights.

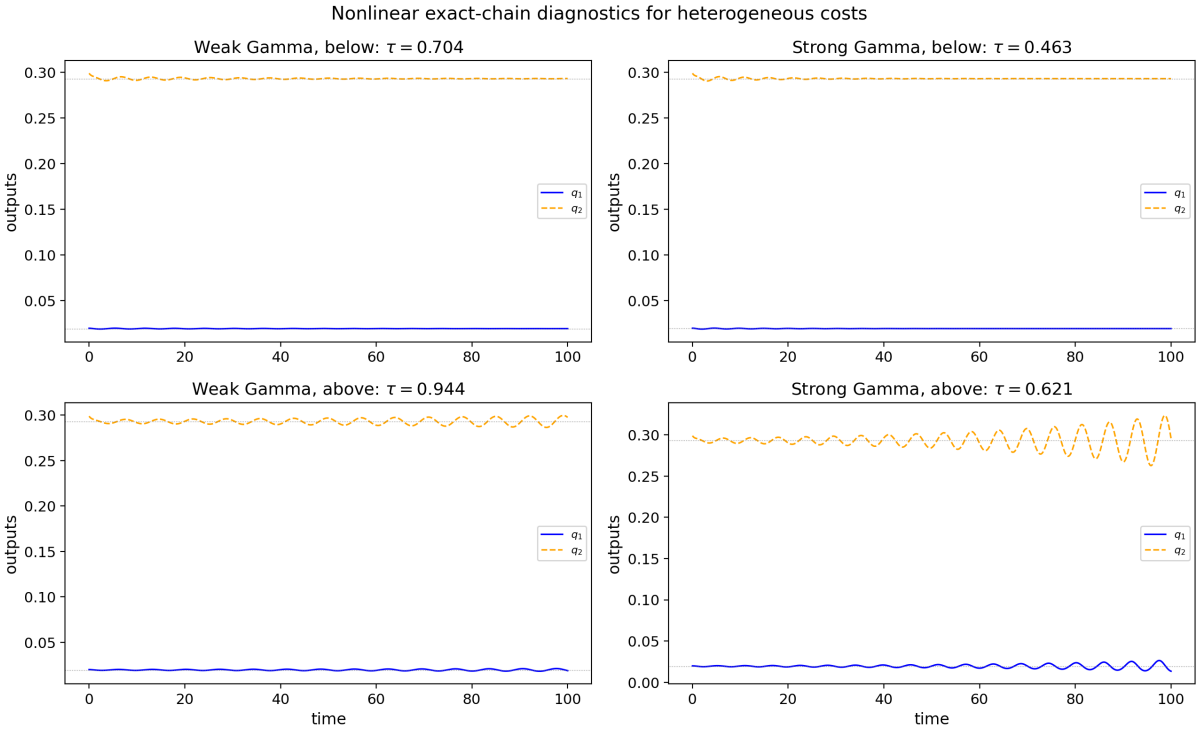


Figure 10: Nonlinear exact-chain diagnostics for heterogeneous costs. Below a crossing the perturbation decays; above it the oscillatory mode grows.

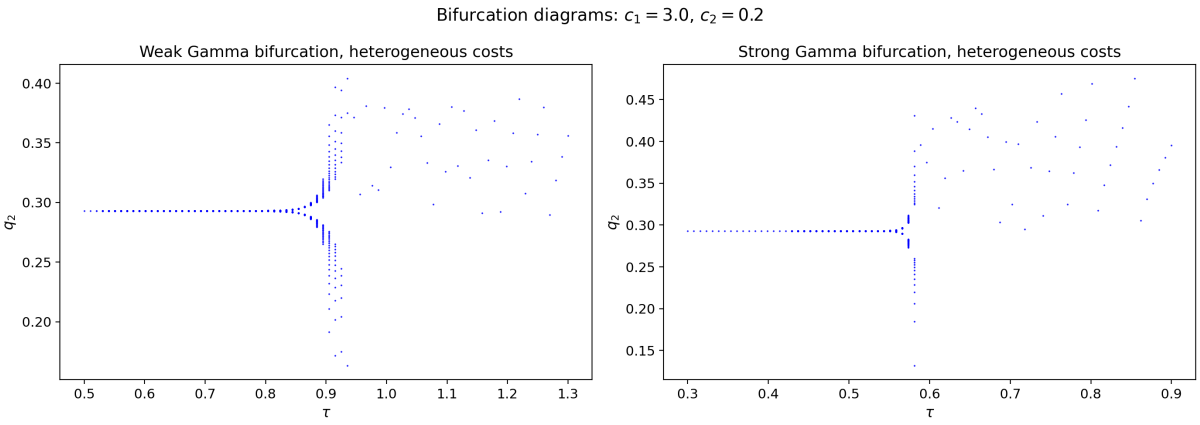


Figure 11: Bifurcation diagrams for weak (left) and strong (right) Gamma chains, heterogeneous costs.

8 Discussion

The analysis yields several insights into the interplay between memory shape and market stability.

Table 6 summarizes the stability properties of all three memory specifications for both the homogeneous and heterogeneous calibrations.

Table 6: Summary of stability results across all specifications.

Specification	Char. eq. degree	Hopf threshold τ^*		Transversality
		Homogeneous	Heterogeneous	
Fixed delay	∞ (transcendental)	1.844	—	Thm 1
Weak Gamma	4 (polynomial)	∞ (none)	0.858	Prop. 4
Strong Gamma	6 (polynomial)	4.696	0.565	Thm 3, Prop. 4

With equal marginal costs, the cross-derivatives b and γ vanish at the equilibrium, so the local problem decomposes into a stable adjustment component (eigenvalue $-A$) and a scalar delayed feedback component. This decomposition makes a complete analytical comparison possible. Among the three homogeneous specifications, the ranking is unambiguous: the fixed point delay is the most destabilizing ($\tau_{\mathrm{d},0} = 1.844$), the strong Gamma kernel postpones the first crossing ($\tau_{\mathrm{s}}^* = 4.696$, a factor of 2.55 larger), and the weak Gamma kernel eliminates the crossing entirely. This confirms and extends the general principle, noted in [31, 32], that distributed delays tend to enhance stability. The economic interpretation is that firms aggregating observations over a range of past dates (distributed memory) generate less volatile adjustment dynamics than firms reacting to a single past observation (point delay). The weak kernel, which assigns exponentially decreasing weight to the past, provides the strongest smoothing effect; the strong kernel, with its hump-shaped profile, provides an intermediate degree of smoothing. Cost heterogeneity ($c_1 \neq c_2$) restores cross-feedback and leads to a genuinely coupled local system. In this setting, no universal closed-form threshold exists. The appropriate theoretical result is conditional and parameter-general: a candidate Hopf point is found from the real and imaginary equations, stability is decided by the relevant Routh–Hurwitz determinants (Table 4), and transversality is verified by (20). The two-parameter stability map (Figure 9) shows that the qualitative ranking, strong kernel more susceptible to instability than weak kernel, persists across a wide range of adjustment speeds and mean delays.

9 Conclusions

This paper has developed a local stability and Hopf-crossing framework for a continuous-time heterogeneous Cournot duopoly in which firms process past market information through distributed memory. Three results stand out.

The first is methodological. By exploiting the linear chain trick, Gamma distributed delays are handled without approximation: the weak and strong memory specifications yield finite-dimensional characteristic polynomials of degree four and six, respectively. This makes the stability analysis considerably more transparent than in the fixed-delay case, where the characteristic equation remains transcendental and admits infinitely many roots.

The second concerns the homogeneous-cost benchmark. When marginal costs coincide, the local system decouples and a complete analytical ranking emerges. The fixed point delay is the most destabilizing specification, the strong Gamma kernel delays the onset of instability by a factor of roughly 2.5, and the weak Gamma kernel eliminates the Hopf crossing entirely, preserving local stability for every mean delay. This demonstrates that replacing a point delay with a distributed memory is not merely a modelling refinement: it changes the stability mechanism itself. Economically, firms that aggregate information gradually generate smoother adjustment

dynamics and are less prone to oscillatory overreaction than firms that respond to a single past observation.

The third concerns heterogeneous costs. Cost asymmetry activates cross-feedback between the two firms, so that universal closed-form thresholds are no longer available. The paper addresses this by deriving exact characteristic equations, Routh–Hurwitz conditions, and a general transversal Hopf test. The numerical analysis then illustrates how these tools work in practice: eigenvalue scans locate the critical delay, root-locus plots confirm the crossing, two-parameter stability maps reveal how the critical region depends on adjustment speed, and nonlinear simulations display the resulting oscillatory dynamics. The qualitative ranking, strong kernel more susceptible to instability than weak kernel, is robust across a wide range of parameters.

Taken together, these results show that the economically relevant object is not only the average time needed to process or implement information, but the entire distribution of memory weights over past observations. A market in which firms react to one sharply dated signal may lose stability much earlier than one in which firms average information gradually, though cost heterogeneity can partially offset this smoothing effect by strengthening cross-firm feedback.

Several extensions present themselves. A normal-form calculation of the first Lyapunov coefficient for the nonlinear chain systems would classify the emerging periodic orbits as supercritical or subcritical. The framework extends naturally to higher-shape Gamma kernels ($n \geq 3$), which produce chains of order n and correspondingly higher-degree characteristic polynomials. Global dynamics, including coexistence of attractors, basin boundaries, and chaotic motion, deserve investigation, especially in the heterogeneous-cost case where the interplay between cost asymmetry and memory shape may generate particularly rich dynamical scenarios. Finally, the empirical calibration of memory kernels from real market data would provide guidance on which region of the parameter space is economically most relevant.

References

[1] Cournot, A.A. (1838). *Recherches sur les principes mathématiques de la théorie des richesses*. Hachette, Paris.

[2] Howroyd, T.D., Russell, A.M. (1984). Cournot oligopoly models with time delays. *Journal of Mathematical Economics*, 13(2), 97–103.

[3] Gori, L., Guerrini, L., Sodini, M. (2015). A continuous time Cournot duopoly with delays. *Chaos, Solitons and Fractals*, 79, 166–177.

[4] Matsumoto, A., Szidarovszky, F. (2014). Discrete and continuous dynamics in nonlinear monopolies. *Applied Mathematics and Computation*, 232, 632–642.

[5] Brianzoni, S., Campisi, G., Guerrini, L. (2018). A continuous-time heterogeneous duopoly model with delays. *Decisions in Economics and Finance*, 41(2), 259–275.

[6] Pecora, N., Sodini, M. (2018). A heterogeneous Cournot duopoly with delay dynamics: Hopf bifurcations and stability switching curves. *Communications in Nonlinear Science and Numerical Simulation*, 58, 36–46.

[7] Matsumoto, A., Szidarovszky, F. (2015). Nonlinear Cournot duopoly with implementation delays. *Chaos, Solitons and Fractals*, 79, 157–165.

[8] Matsumoto, A., Szidarovszky, F. (2012). Nonlinear delay monopoly with bounded rationality. *Chaos, Solitons and Fractals*, 45(4), 507–519.

[9] Matsumoto, A., Szidarovszky, F. (2018). *Dynamic Oligopolies with Time Delays*. Springer, Singapore.

[10] Agiza, H.N., Elsadany, A.A. (2003). Nonlinear dynamics in the Cournot duopoly game with heterogeneous players. *Physica A*, 320, 512–524.

[11] Bischi, G.I., Naimzada, A.K., Sbragia, L. (2007). Oligopoly games with local monopolistic approximation. *Journal of Economic Behavior and Organization*, 62(3), 371–388.

[12] Bischi, G.I., Lamantia, F., Radi, D. (2015). An evolutionary Cournot model with limited market knowledge. *Journal of Economic Behavior and Organization*, 116, 219–238.

[13] Puu, T. (1995). The chaotic monopolist. *Chaos, Solitons and Fractals*, 5(1), 35–44.

[14] Tramontana, F. (2010). Heterogeneous duopoly with isoelastic demand function. *Economic Modelling*, 27(1), 350–357.

[15] Ahmed, R., Qureshi, M.Z.A., Abbas, M., Mumtaz, N. (2025). Bifurcation and chaos control in a heterogeneous Cournot–Bertrand duopoly game model. *Chaos, Solitons and Fractals*, 190, 115757.

[16] Lamantia, F., Radi, D., Tichý, T. (2025). Two-population evolutionary oligopoly with partial cooperation and partial hostility. *Computational Economics*, 65(2), 763–794.

[17] Wei, Z., Tan, W., Elsadany, A.A., Moroz, I. (2023). Complexity and chaos control in a Cournot duopoly model based on bounded rationality and relative profit maximization. *Nonlinear Dynamics*, 111(18), 17561–17589.

[18] Cavalli, F., Naimzada, A., Tramontana, F. (2015). Nonlinear dynamics and global analysis of a heterogeneous Cournot duopoly with a local monopolistic approach versus a gradient rule with endogenous reactivity. *Communications in Nonlinear Science and Numerical Simulation*, 23, 245–262.

[19] Matsumoto, A., Szidarovszky, F. (2025). Asymptotic dynamics in a multi-market delayed cobweb model. *Computational Economics*, 65(2), 877–912.

[20] Mignot, S., Tramontana, F., Westerhoff, F. (2024). Complex dynamics in a nonlinear duopoly model with heuristic expectation formation and learning behavior. *Annals of Operations Research*, 337(3), 809–834.

[21] Bischi, G.I., Cerboni Baiardi, L., Lamantia, F., Radi, D. (2024). Nonlinear dynamics and game-theoretic modeling in economics and finance. *Annals of Operations Research*, 337(3), 731–737.

[22] Hassard, B.D., Kazarinoff, N.D., Wan, Y.-H. (1981). *Theory and Applications of Hopf Bifurcation*. Cambridge University Press.

[23] Hale, J.K., Verduyn Lunel, S.M. (1993). *Introduction to Functional Differential Equations*. Springer-Verlag.

[24] Gu, K., Niculescu, S.-I., Chen, J. (2005). On stability crossing curves for general systems with two delays. *Journal of Mathematical Analysis and Applications*, 311(1), 231–253.

[25] Beretta, E., Kuang, Y. (2002). Geometric stability switch criteria in delay differential systems with delay dependent parameters. *SIAM Journal on Mathematical Analysis*, 33(5), 1144–1165.

[26] Guerrini, L., Matsumoto, A., Szidarovszky, F. (2018). Delay Cournot duopoly models revisited. *Chaos*, 28(9), 093113.

[27] Cao, Y., Colucci, R., Guerrini, L. (2022). On the stability analysis of a delayed two-stage Cournot model with R&D spillovers. *Mathematics and Computers in Simulation*, 201, 543–554.

[28] Dieci, R., Mignot, S., Westerhoff, F. (2022). Production delays, technology choice and cyclical cobweb dynamics. *Chaos, Solitons and Fractals*, 156, 111874.

[29] Fargue, D.M. (1973). Réducibilité des systèmes héréditaires à des systèmes dynamiques. *Comptes Rendus de l'Académie des Sciences Paris*, 277B, 471–473.

[30] MacDonald, N. (1978). *Time Lags in Biological Models*. Springer-Verlag.

[31] Kuang, Y. (1993). *Delay Differential Equations with Applications in Population Dynamics*. Academic Press.

[32] Smith, H.L. (2011). An introduction to delay differential equations with applications to the life sciences. Springer.

[33] Diekmann, O., Gyllenberg, M., Metz, J.A.J. (2018). Finite dimensional state representation of linear and nonlinear delay systems. *Journal of Dynamics and Differential Equations*, 30(4), 1439–1467.

[34] Hurtado, P.J., Kirosingh, A.S. (2019). Generalizations of the linear chain trick. *Journal of Mathematical Biology*, 79(5), 1831–1883.

[35] Cassidy, T., Gillich, P., Humphries, A.R., van Dorp, C.H. (2022). Numerical methods and hypoexponential approximations for gamma-distributed delay differential equations. *IMA Journal of Applied Mathematics*, 87(6), 1043–1089.

[36] Castro, M.Á., García, M.A., Martín, J.A., Rodríguez, F. (2024). Delay effects on plant stability and symmetry-breaking pattern formation in a Klausmeier–Gray–Scott model of semiarid vegetation. *Symmetry*, 16(5), 609.

[37] Gori, L., Guerrini, L., Sodini, M. (2017). A characterisation of duopoly dynamics with frictions in production adjustments. *Journal of Evolutionary Economics*, 27(5), 963–988.

[38] Gori, L., Guerrini, L., Sodini, M. (2015). Hopf bifurcation and stability crossing curves in a cobweb model with heterogeneous producers and time delays. *Nonlinear Analysis: Hybrid Systems*, 18, 117–133.

[39] Culda, L.C., Kaslik, E., Neamţu, M. (2022). Stability and bifurcations in a general Cournot duopoly model with distributed time delays. *Chaos, Solitons and Fractals*, 162, 112424.

[40] Bianca, C., Guerrini, L., Ragni, S. (2025). Delayed energy demand–supply models with gamma-distributed memory kernels. *AppliedMath*, 5(4), 162.

[41] Wang, N., Gu, K., Liu, Z., Xu, C. (2025). Dynamical analysis of a fractional-order Cournot–Bertrand duopoly model with time delays. *AIMS Mathematics*, 10(8), 17567–17601.

[42] Culda, L.C., Kaslik, E., Neamţu, M., Sîrghi, N. (2024). Dynamics of a discrete-time mixed oligopoly Cournot-type model with three time delays. *Mathematics and Computers in Simulation*, 226, 524–539.

[43] Corless, R.M., Gonnet, G.H., Hare, D.E.G., Jeffrey, D.J., Knuth, D.E. (1996). On the Lambert W function. *Advances in Computational Mathematics*, 5, 329–359.